Supporting Information

Design Principles of Biphenylene-Supported Dual-Atom Catalysts for Efficient and Selective Nitrate Reduction to Ammonia

Kiruthika Pandiyan, and Hsin-Tsung Chen*

Department of Chemistry, Research Center for Semiconductor Materials and Advanced Optics, and R&D Center for Membrane Technology, Chung Yuan Christian University, Chungli District, Taoyuan City 320314, Taiwan

*Corresponding author. E-mail: htchen@cycu.edu.tw; Tel: +886-3-265-3324

Note S1. Elementary and kinetic steps of NO_3RR

Electrochemical reduction of NO_3^- results in the formation of NH_3 with nine protons and eight electrons transferred. The whole reaction can be summarized as

$$NO_3^- + 9H^+ + 8e^- \rightarrow NH_3 + 3H_2O \quad (R1)$$

Involving the intermediates $*NO_3$, $*NO_3H$, $*NO_2$, $*NO_2H$, $*NO$, $*NOH$, $*N$, $*NH$, $*NH_2$ and $*NH_3$, N-end and NO-side pathways are considered as the most favorable pathway on TM_2@BPN and the elementary steps of these pathways are described as follows:

$$* + NO_3^- \rightarrow *NO_3 + e^- \quad (R2)$$

$$*NO_3 + H^+ + e^- \rightarrow *NO_3H \quad (R3)$$

$$*NO_3H + H^+ + e^- \rightarrow *NO_2 + H_2O \quad (R4)$$

$$*NO_2 + H^+ + e^- \rightarrow *NO_2H \quad (R5)$$

$$*NO_2H + H^+ + e^- \rightarrow *NO + H_2O \quad (R6)$$

N-end pathway

$$*NO + H^+ + e^- \rightarrow *NOH \quad (R7)$$

$$*NOH + H^+ + e^- \rightarrow *N + H_2O \quad (R8)$$

$$*N + H^+ + e^- \rightarrow *NH \quad (R9)$$

NO-side pathway

$$**NO + H^+ + e^- \rightarrow **NOH \quad (R10)$$

$$**NOH + H^+ + e^- \rightarrow **NHOH \quad (R11)$$

$$**NOH + H^+ + e^- \rightarrow **NH_2O \quad (R12)$$

$$**NHOH + H^+ + e^- \rightarrow **NH_2OH \quad (R13)$$

$$**NHOH + H^+ + e^- \rightarrow *NH + H_2O \quad (R14)$$

$$*NH + H^+ + e^- \rightarrow *NH_2 \quad (R15)$$

$$**NH_2OH + H^+ + e^- \rightarrow **NH_2 + H_2O \quad (R16)$$

$$*NH_2 + H^+ + e^- \rightarrow *NH_3 \quad (R17)$$

$$*NH_3 \rightarrow * + NH_3 \qquad (R18)$$

The ΔG between two states involve in the NO_3RR reduction process can be expressed as to:

$\Delta G = G(NO_{3-m}H_n) + m\,G(H_2O) - G(NO_3^-) - n/2\,G(H_2) - G(*)$

where * denotes the surface of TM_2@BPN, n is the number of H^+/e^- pairs transferred, and m (m=0, 1,2,3) is the number of H_2O molecules released. Thus,

$\Delta G(*NO_3H) = G(*NO_3H) - G(*) - G(NO_3^-) - 1/2G(H_2)$

$\Delta G(*NO_2) = G(*NO_2) - G(*) - G(NO_3^-) - G(H_2) + G(H_2O)$

$\Delta G(*NO_2H) = G(*NO_2H) - G(*) - G(NO_3^-) - 3/2G(H_2) + G(H_2O)$

$\Delta G(*NO) = G(*NO) - G(*) - G(NO_3^-) - 2G(H_2) + 2G(H_2O)$

$\Delta G(*NOH) = G(*NOH) - G(*) - G(NO_3^-) - 5/2G(H_2) + 2G(H_2O)$

$\Delta G(*N) = G(*N) - G(*) - G(NO_3^-) - 3G(H_2) + 3G(H_2O)$

$\Delta G(**NHOH) = G(**NHOH) - G(*) - G(NO_3^-) - 3G(H_2) + 2G(H_2O)$

$\Delta G(**NH_2O) = G(**NH_2O) - G(*) - G(NO_3^-) - 3G(H_2) + 2G(H_2O)$

$\Delta G(**NH_2OH) = G(**NH_2OH) - G(*) - G(NO_3^-) - 7/2G(H_2) + 2G(H_2O)$

$\Delta G(*NH) = G(*NH) - G(*) - G(NO_3^-) - 7/2G(H_2) + 3G(H_2O)$

$\Delta G(*NH_2) = G(*NH_2) - G(*) - G(NO_3^-) - 4G(H_2) + 3G(H_2O)$

$\Delta G(*NH_3) = G(*NH_3) - G(*) - G(NO_3^-) - 9/2G(H_2) + 3G(H_2O)$

For example, if we consider the rate-determining step of Rh_2@BPN

1. $\Delta G(*NO) = G(*NO) - G(Rh_2@BPN) - G(NO_3^-) - 2G(H_2) + 2G(H_2O)$

$G(*NO) = -499.8132972$, $G(Rh_2@BPN) = -484.3864813$, $G(NO_3^-) = -24.91378556$, $G(H_2) = -6.9$

$G(H_2O) = -14.32$

$\Delta G(*NO) = -499.8132972 - (-484.3864813) - (-24.91378556) - 2(-6.9) + 2(-14.32)$

ΔG(*NO) = -5.353 eV

2. ΔG(*NOH) = G(*NOH) - G(Rh_2@BPN) - G(NO_3^-) – 5/2G(H_2) + 2G(H_2O)

G(*NOH) = -503.0984867

ΔG(*NOH) = -503.0984867- (-484.3864813) – (-24.91378556) – 5/2(-6.9) + 2 (-14.32)

ΔG(*NOH) = **-5.188 eV**

The relative energy is ΔG(*NOH) - ΔG(*NO) = -5.188 – (-5.353) **= 0.16 eV**

Consider the rate-determining step of Os_2@BPN

1. ΔG(*NO) = G(*NO) - G(Os_2@BPN) - G(NO_3^-) – 2G(H_2) + 2G(H_2O)

G(*NO) = -504.004074, G(Os_2@BPN) = -489.0776676, G(NO_3^-) = -24.91378556, G(H_2) = -6.9

G(H_2O) = -14.32

ΔG(*NO) = -504.004074 - (-489.0776676) – (-24.91378556) – 2(-6.9) + 2 (-14.32)

ΔG(*NO) = -4.852 eV

2. ΔG(*NOH) = G(*NOH) - G(Os_2@BPN) - G(NO_3^-) – 5/2G(H_2) + 2G(H_2O)

G(*NOH) = -507.1287723

ΔG(*NOH) = -507.1287723- (-489.0776676) – (-24.91378556) – 5/2(-6.9) + 2 (-14.32)

ΔG(*NOH) = **-4.527 eV**

The relative energy is ΔG(*NOH) - ΔG(*NO) = -4.527 – (-4.852) **= 0.32 eV**

The kinetic steps of NO_3RR on Rh_2@BPN and Os_2@BPN

However, in Figures S11 and S12, we performed nudged elastic band calculations for *NO + ($H_3O^+ + e^-$) → *NOH + H_2O on Rh_2@BPN and *NO + ($H_3O^+ + e^-$) → *NOH + H_2O on Os_2@BPN.

So, the energy difference is calculated by

ΔE = E(*HNO + H_2O) – E(*NO + ($H_3O^+ + e^-$)) for Rh_2@BPN

= -515.6195836 – (-512.90064229)

= **-2.72 eV**

ΔE = E(*NOH + H_2O) – E(*NO + ($H_3O^+ + e^-$)) for OS_2@BPN

= -519.3878837 – (-516.9307566)

= **-2.46 eV**

Note S2. Solvent effect

Specifically, we employed the implicit solvation model VASPsol, (1) to simulate aqueous conditions. Due to the computational cost we have chosen best catalyst (Rh_2@BPN, Os_2@BPN) from our study. The results obtained from calculations, are as summarized in Table S17 and S18. The results show that solvation alters the limiting potential by 0.08 and 0.03 V. However, previous studies report that solvent effects on NO_3RR are minor and have often been neglected. Accordingly, solvation effects are omitted in this work. (2-4).

Reference

1. K. Mathew, R. Sundararaman, K. Letchworth-Weaver, T. A. Arias and R. G. Hennig, J. Chem. Phys., 2014, 140.

2. H. Niu, Z. Zhang, X. Wang, X. Wan, C. Shao and Y. Guo, Adv. Funct. Mater., 2021, 31, 2008533.

3. T. Zhao, K. Chen, X. Xu, X. Li, X. Zhao, Q. Cai, K. Chu and J. Zhao, Appl. Catal. B: Environ., 2023, 339, 123156.

4. X. Guo, J. Gu, S. Lin, S. Zhang, Z. Chen and S. Huang, J. Am. Chem. Soc., 2020, 142, 5709-5721.

Note S3. Faradaic efficiency

The following equation estimates the theoretical Faradaic efficiencies (FE) and quantitatively represents the NO_3RR selectivity on TM_2@BPN.

$$FE = \left[\frac{1}{(1+e^{-\Delta G/k_B T}}\right]$$

Where ΔG represents the difference in free energy of the potential determining step between the HER and NO_3RR, k_B represents the Boltzmann constant (8.617×10^{-5} eV K^{-1}), and T represents the room temperature (298.15 K). The theoretical formula for Faradaic efficiency employed in this study was adapted from recently published works.(1-5) These studies established the theoretical framework in which the hydrogen evolution reaction (HER) is treated as the primary competing process against NO_3RR and the corresponding statistical model is derived based on the following assumptions: (1) the mass and electron transfer are not the rate determining factors for both HER and NO_3RR (2) only HER and NO_3RR are competing reactions, and (3) the selectivity of NO_3RR in comparison to HER could be estimated by Boltzmann distribution. Under these assumptions, the adopted formula offers a feasible theoretical approach for evaluating FE in NO_3RR. The total FE values approaching 100% should be regarded as theoretical probabilities before normalization, reflecting the potential tendency of each reaction under the given conditions. As experimental calibration data are not yet available, the FE values presented in Table S16 serve as theoretical references for future experimental validation.

Reference

1. W. Zhao, L. Zhang, Q. Luo, Z. Hu, W. Zhang, S. Smith and J. Yang, ACS Catal., 2019, 9, 3419-3425.

2. X. Liu, Y. Jiao, Y. Zheng, M. Jaroniec and S.-Z. Qiao, J. Am. Chem. Soc., 2019, 141, 9664-9672.

3. N. Sathishkumar and H.-T. Chen, J. Phys. Chem. C., 2023, 127, 994-1005.

4. D. Jiao, Y. Liu, Q. Cai and J. Zhao, J. Mater. Chem. A., 2021, 9, 1240-1251.

5. X. Lv, W. Wei, B. Huang, Y. Dai and T. Frauenheim, Nano Letters, 2021, 21, 1871-1878.

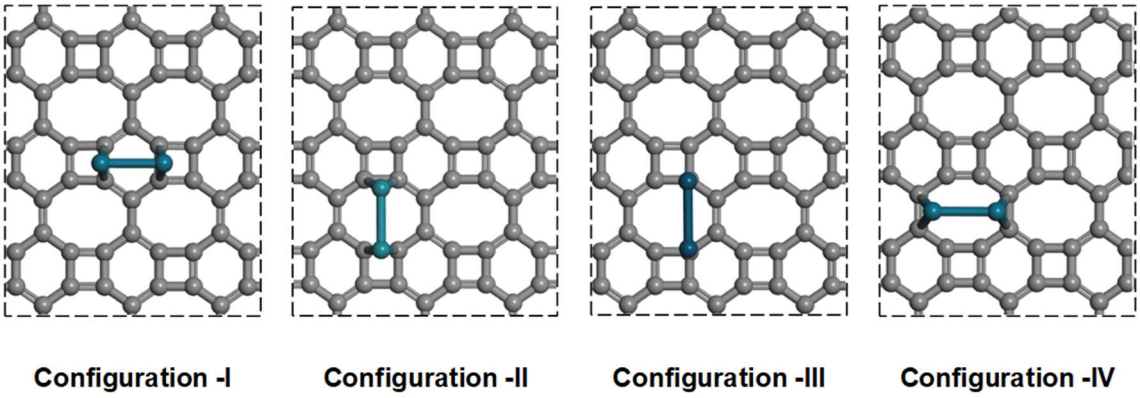

Figure S1. Four possible binding configurations of TM dimer on BPN.

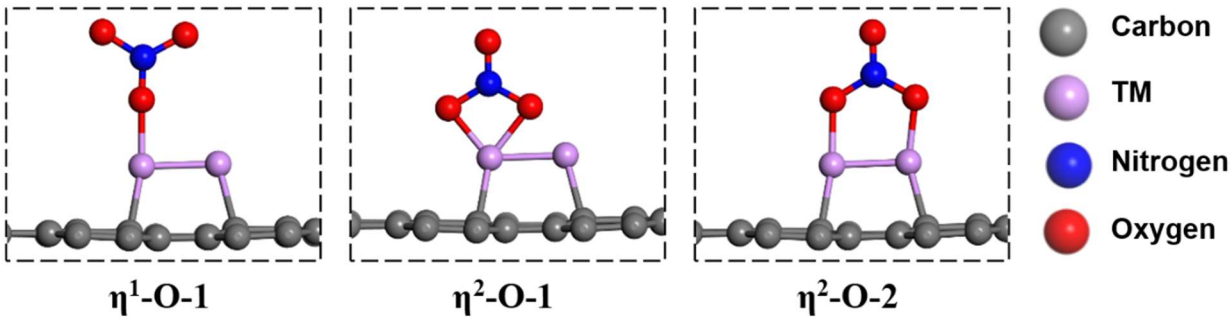

Figure S2. Three possible adsorption configurations of NO_3^- on TM_2@BPN.

(a)

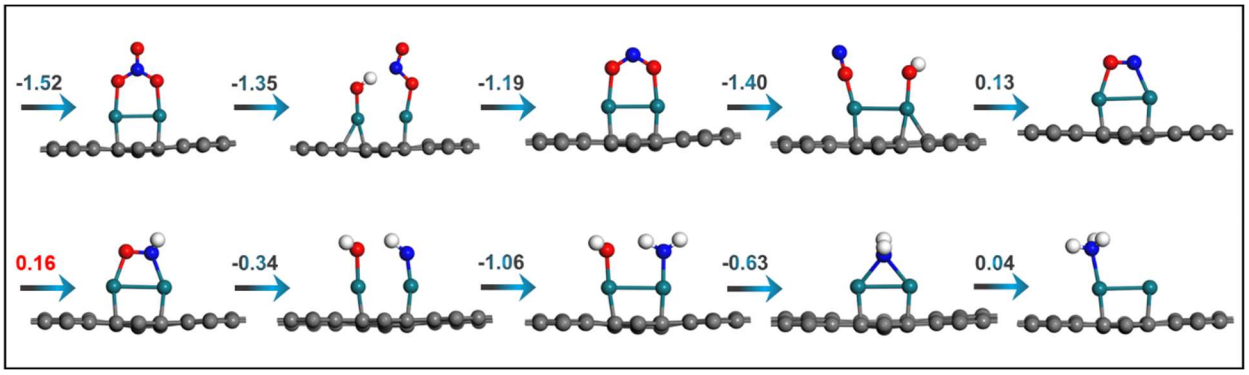

(b)

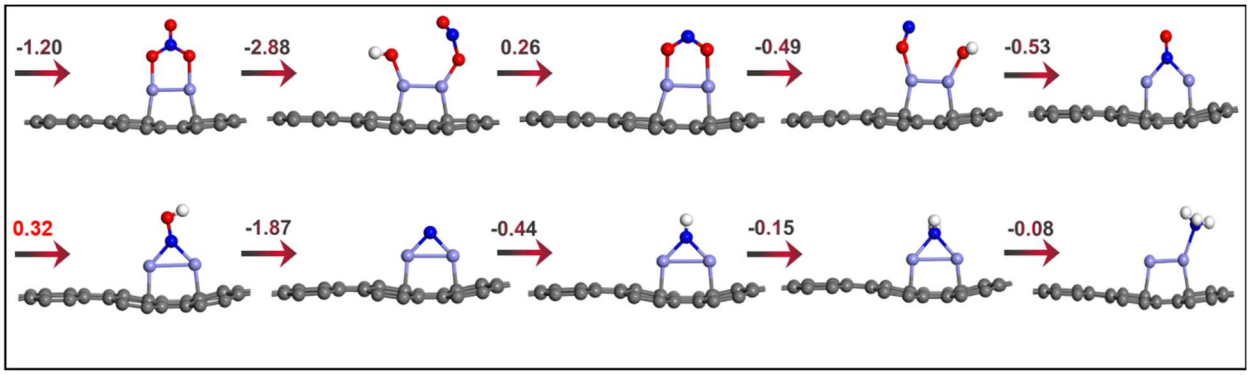

(c)

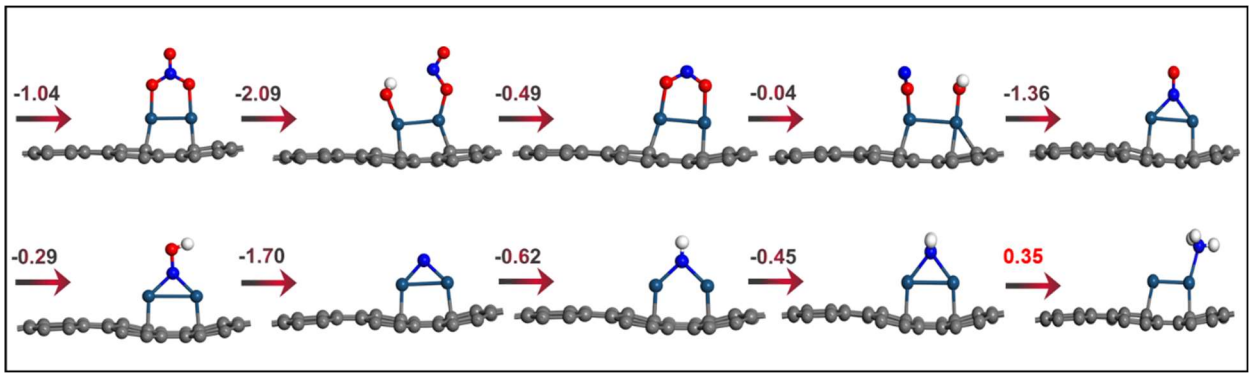

Figure S3 (a-c). DFT-optimized configurations of intermediates associated with free energy diagram of Rh_2@BPN, Os_2@BPN and Ir_2@BPN respectively.

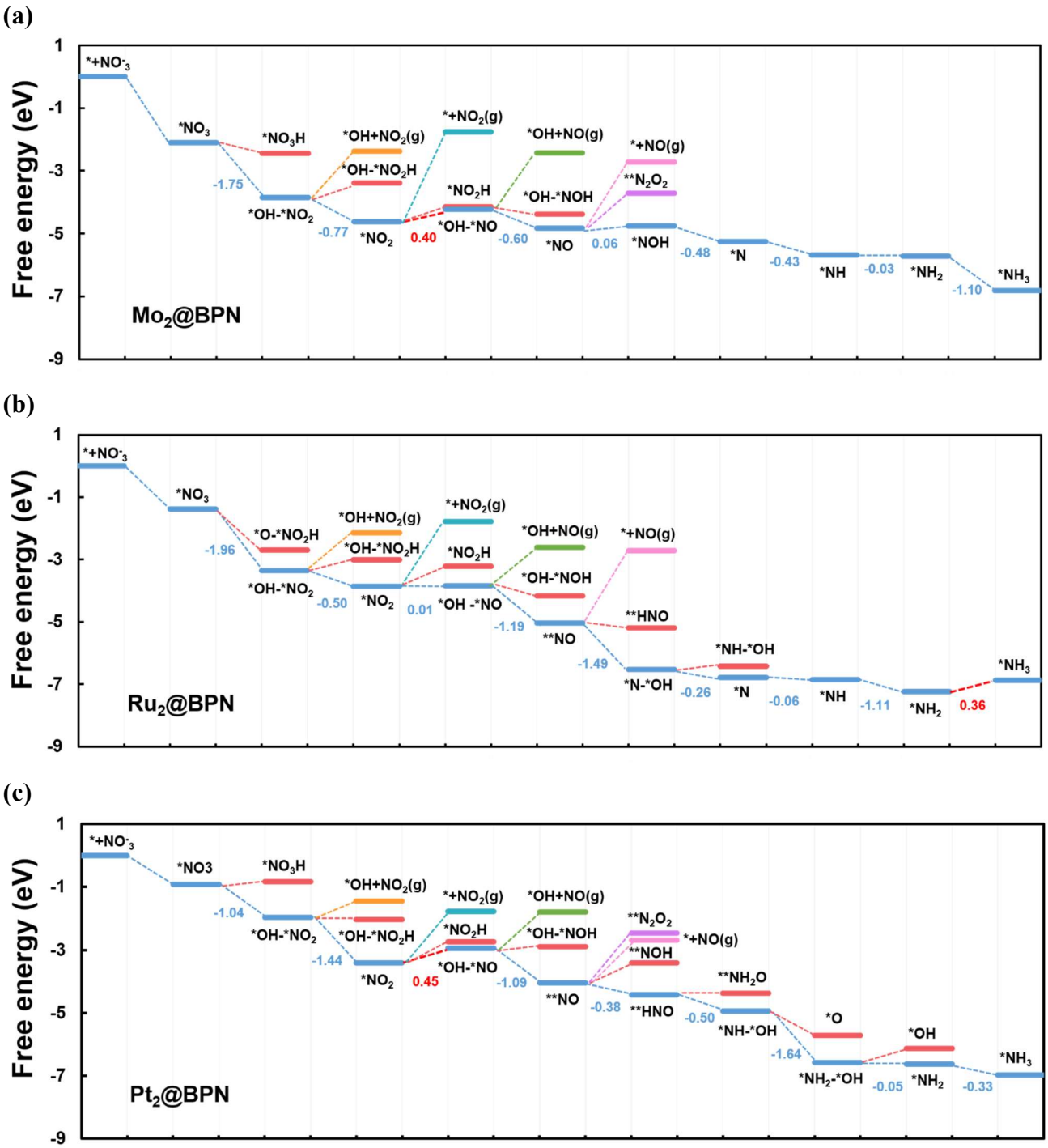

Figure S4 (a-c). Free energy diagram for NO_3RR on Mo_2@BPN, Ru_2@BPN and Pt_2@BPN catalysts respectively. (U_L > -0.5V)

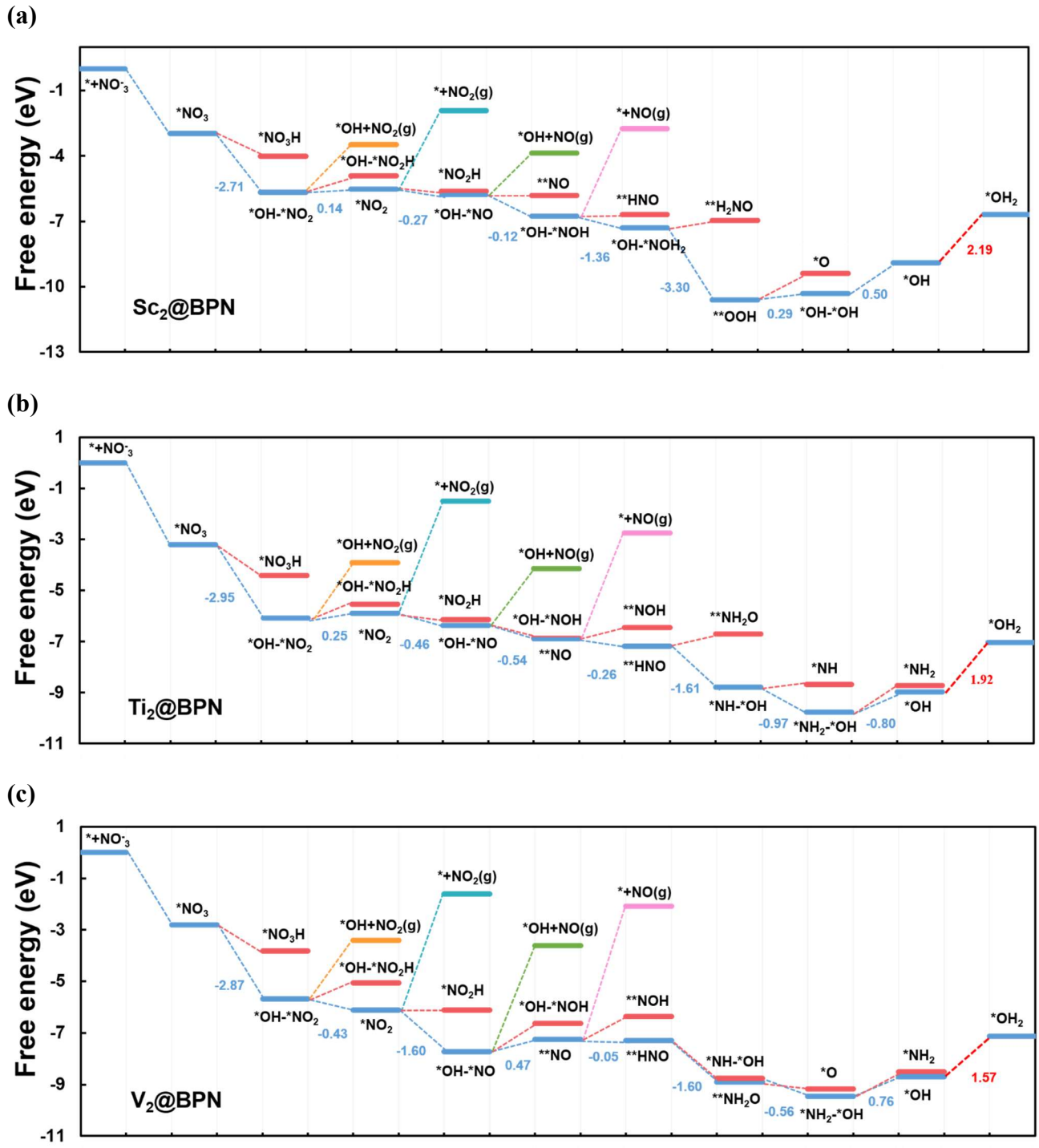

Figure S5 (a-c). Free energy diagram for NO_3RR on Sc_2@BPN, Ti_2@BPN and V_2@BPN catalysts respectively.

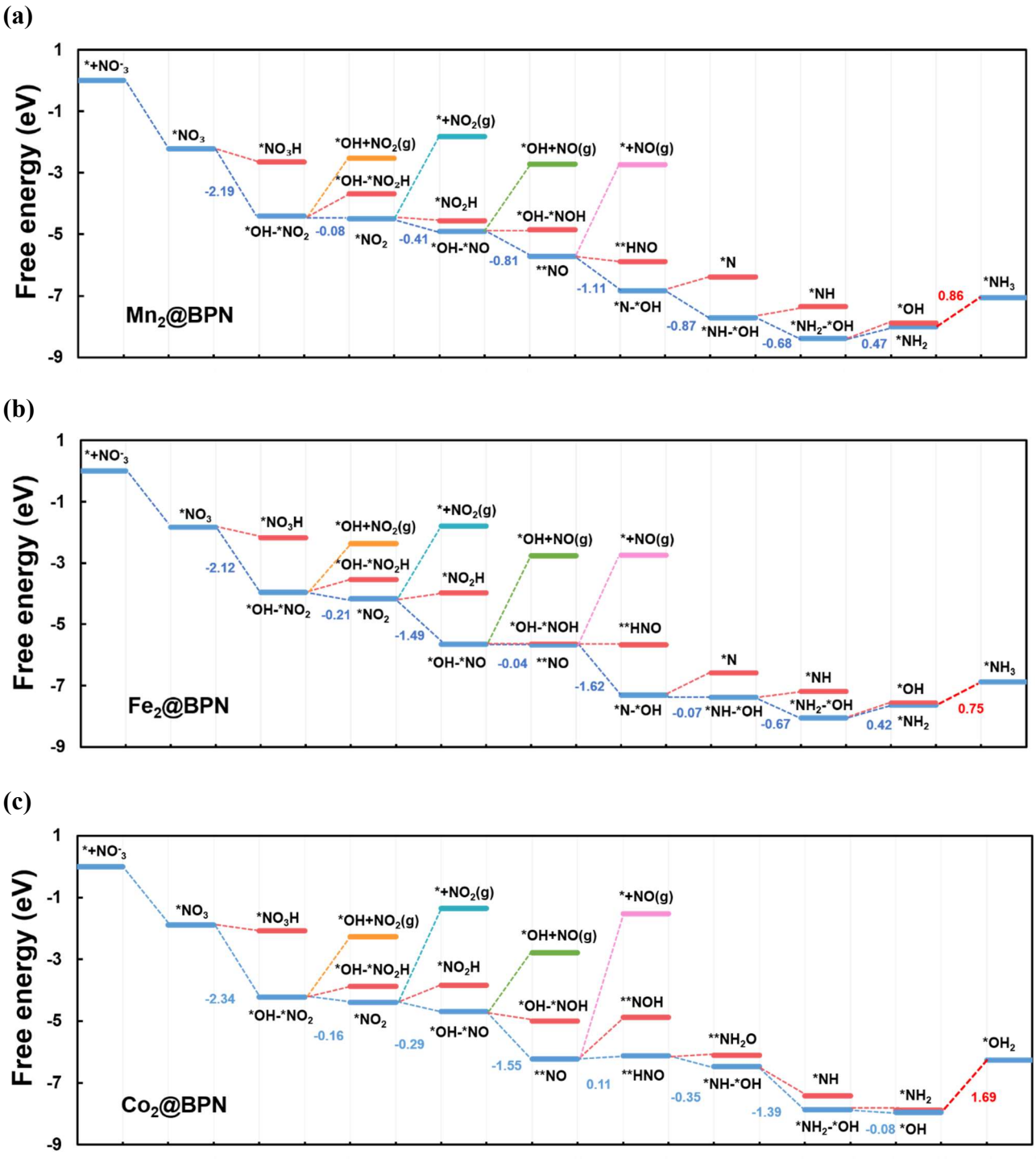

Figure S6 (a-c). Free energy diagram for NO_3RR on Mn_2@BPN, Fe_2@BPN and Co_2@BPN catalysts respectively.

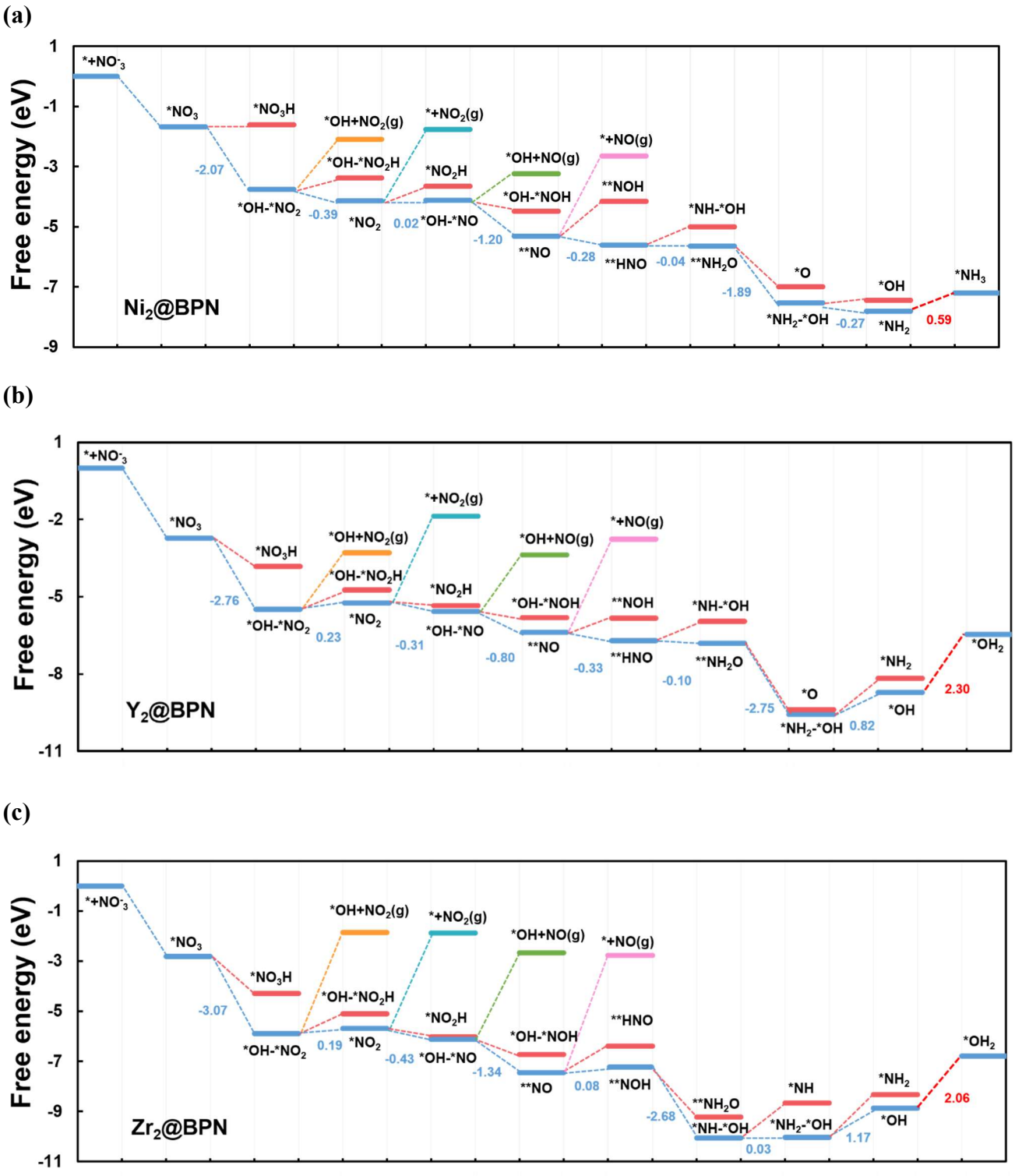

Figure S7 (a-c). Free energy diagram for NO_3RR on Ni_2@BPN, Y_2@BPN and Zr_2@BPN catalysts respectively.

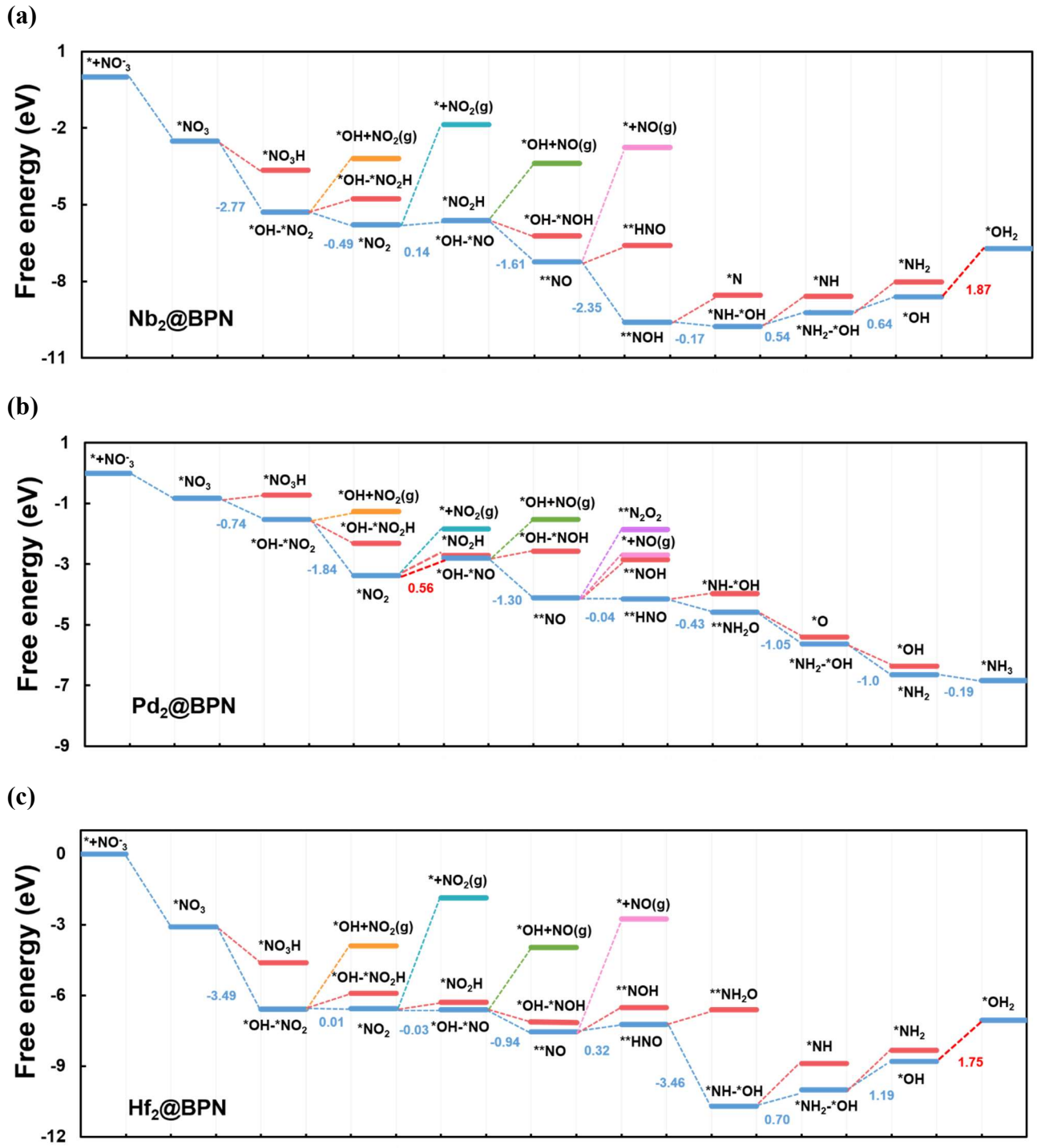

Figure S8 (a-c). Free energy diagram for NO_3RR on Nb_2@BPN, Pd_2@BPN and Hf_2@BPN catalysts respectively.

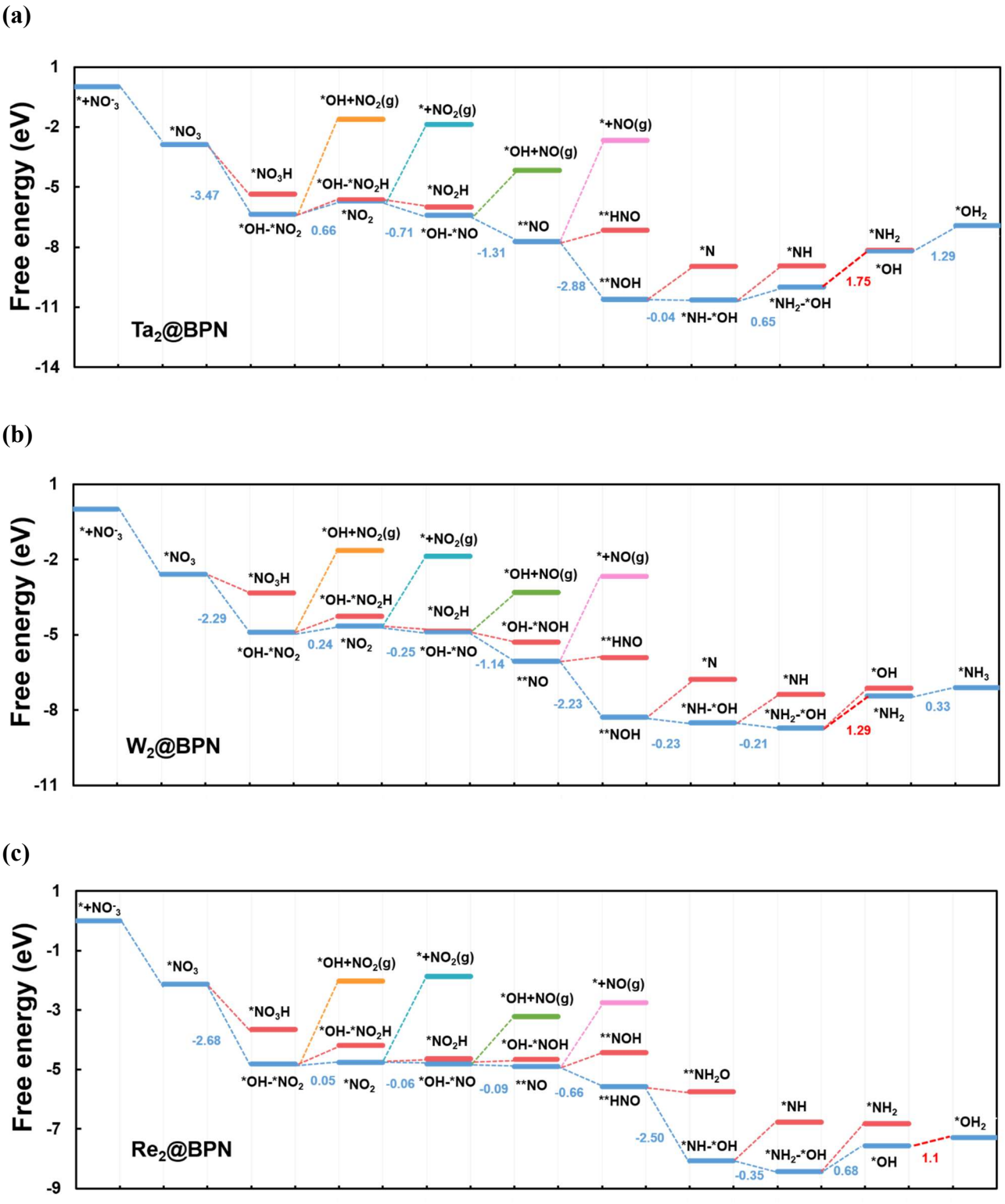

Figure S9 (a-c). Free energy diagram for NO_3RR on Ta_2@BPN, W_2@BPN and Re_2@BPN catalysts respectively.

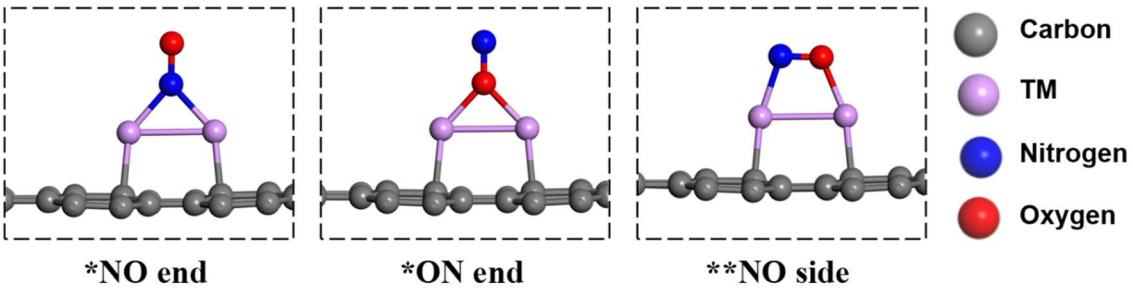

Figure S10. Three possible adsorption configurations of NO on TM_2@BPN.

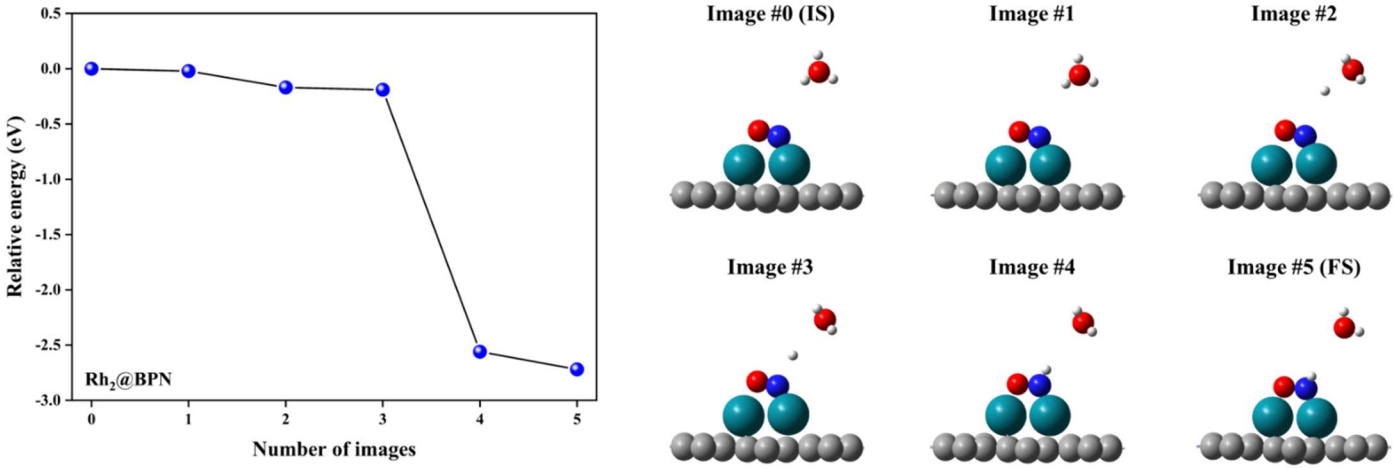

Figure S11. Nudged elastic band calculation results for *NO + (H_3O^+ + e^-) → *NOH + H_2O on Rh_2@BPN.

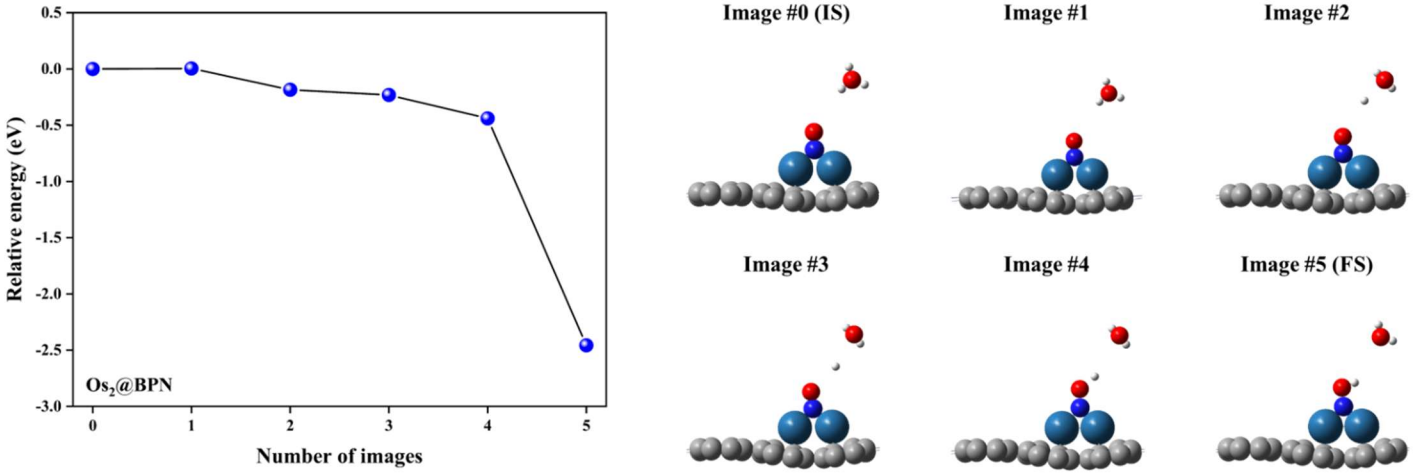

Figure S12. Nudged elastic band calculation results for *NO + (H_3O^+ + e^-) → *NOH + H_2O on Os_2@BPN.

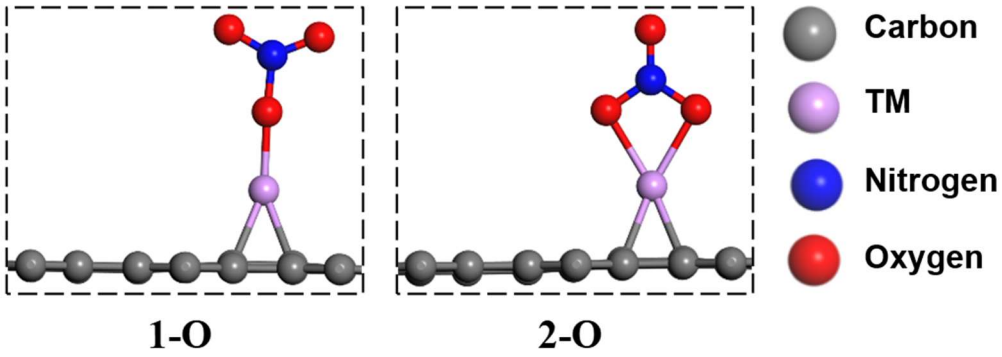

Figure S13. Two possible adsorption configurations of NO_3^- on TM@BPN.

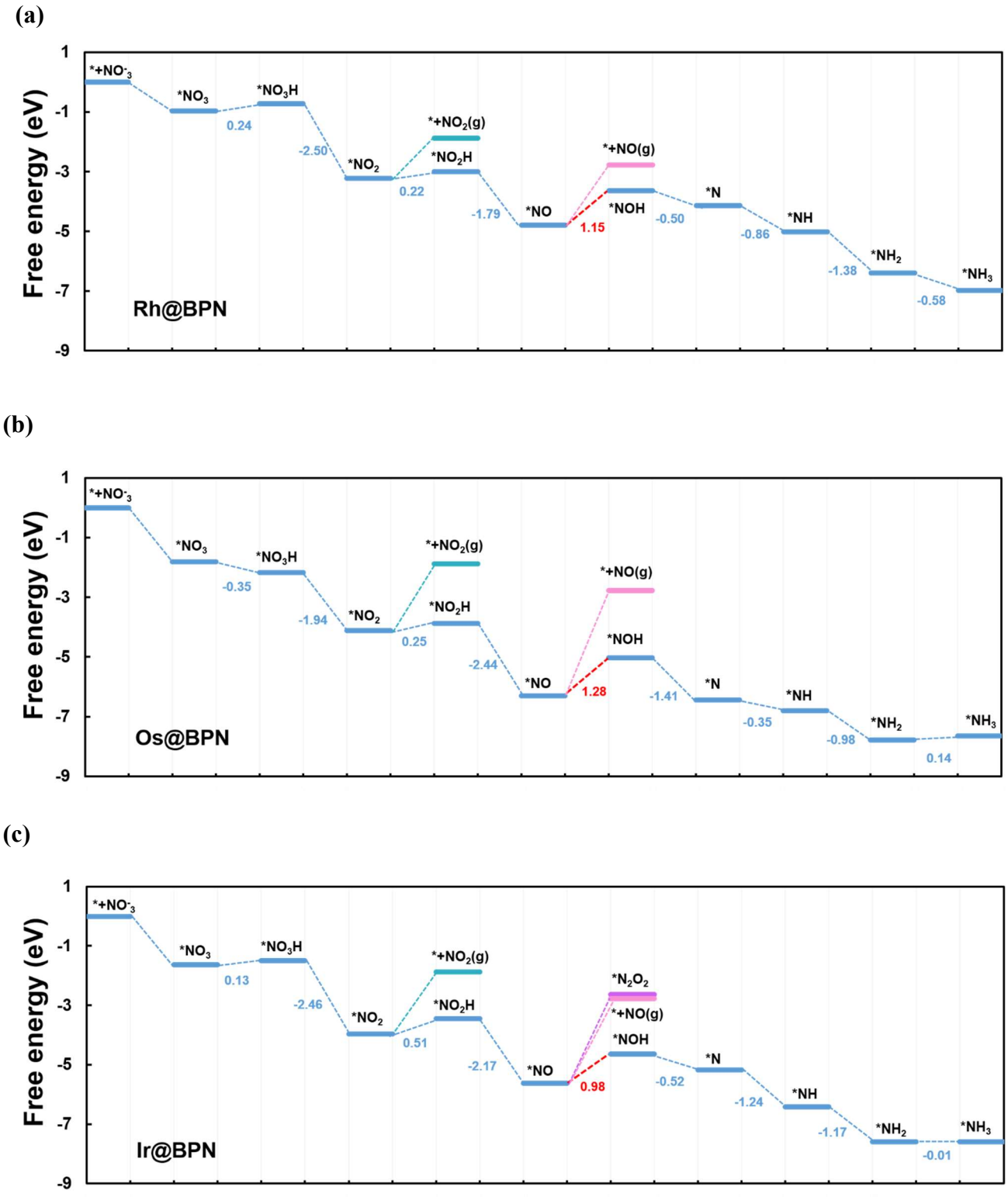

Figure S14 (a-c). Free energy diagram for NO_3RR on Rh@BPN, Os@BPN and Ir@BPN SACs catalysts respectively.

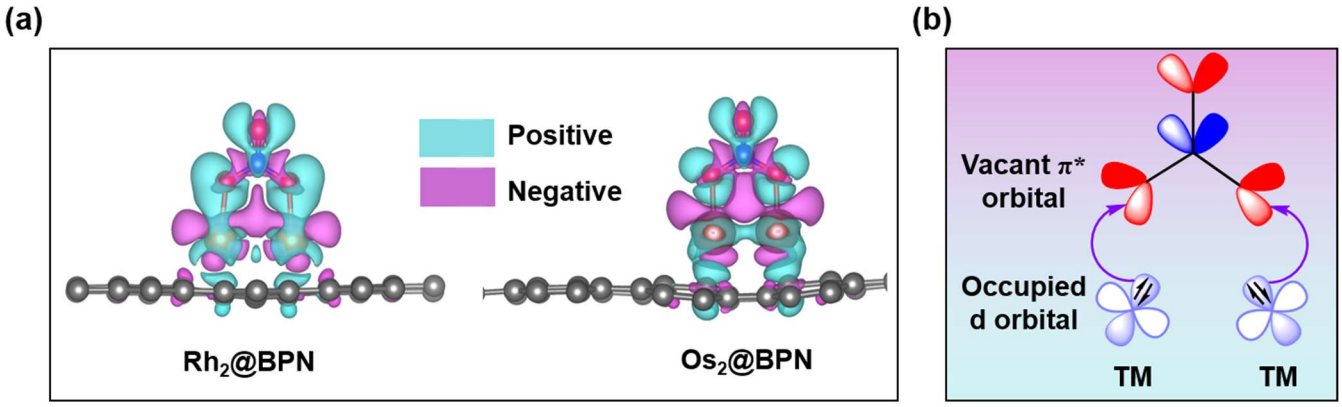

Figure S15 (a) Charge density differences of nitrate adsorbed on Rh_2@BPN, and Os_2@BPN the isosurface value is 0.001 e /Å^3. **(b)** Schematic representation of the nitrate adsorption mechanism on the TM dimer.

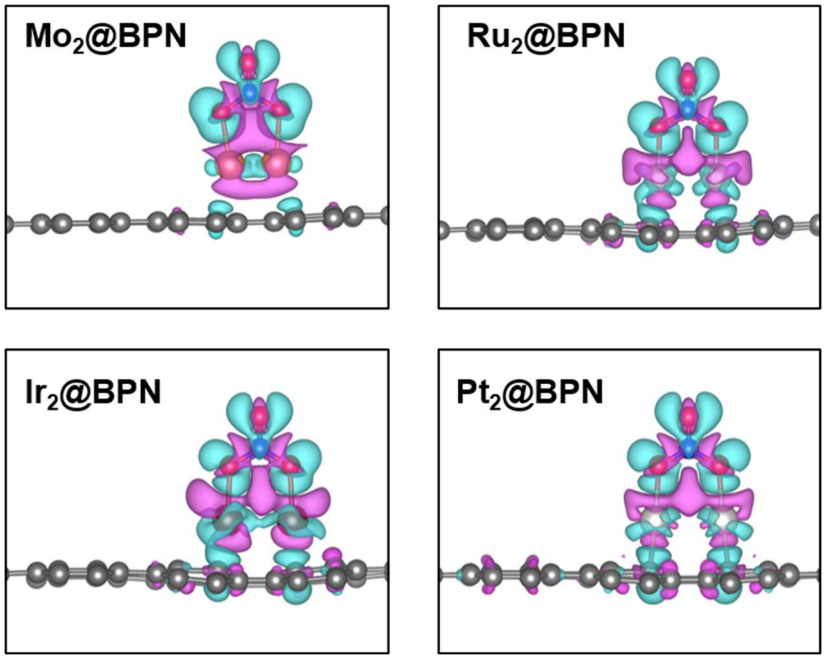

Figure S16. Charge density differences of nitrate adsorbed on Mo_2@BPN, Ru_2@BPN, Ir_2@BPN and Pt_2@BPN, the isosurface value is 0.001 e /Å^3. The charge depletion and accumulation were depicted by cyan and violet respectively.

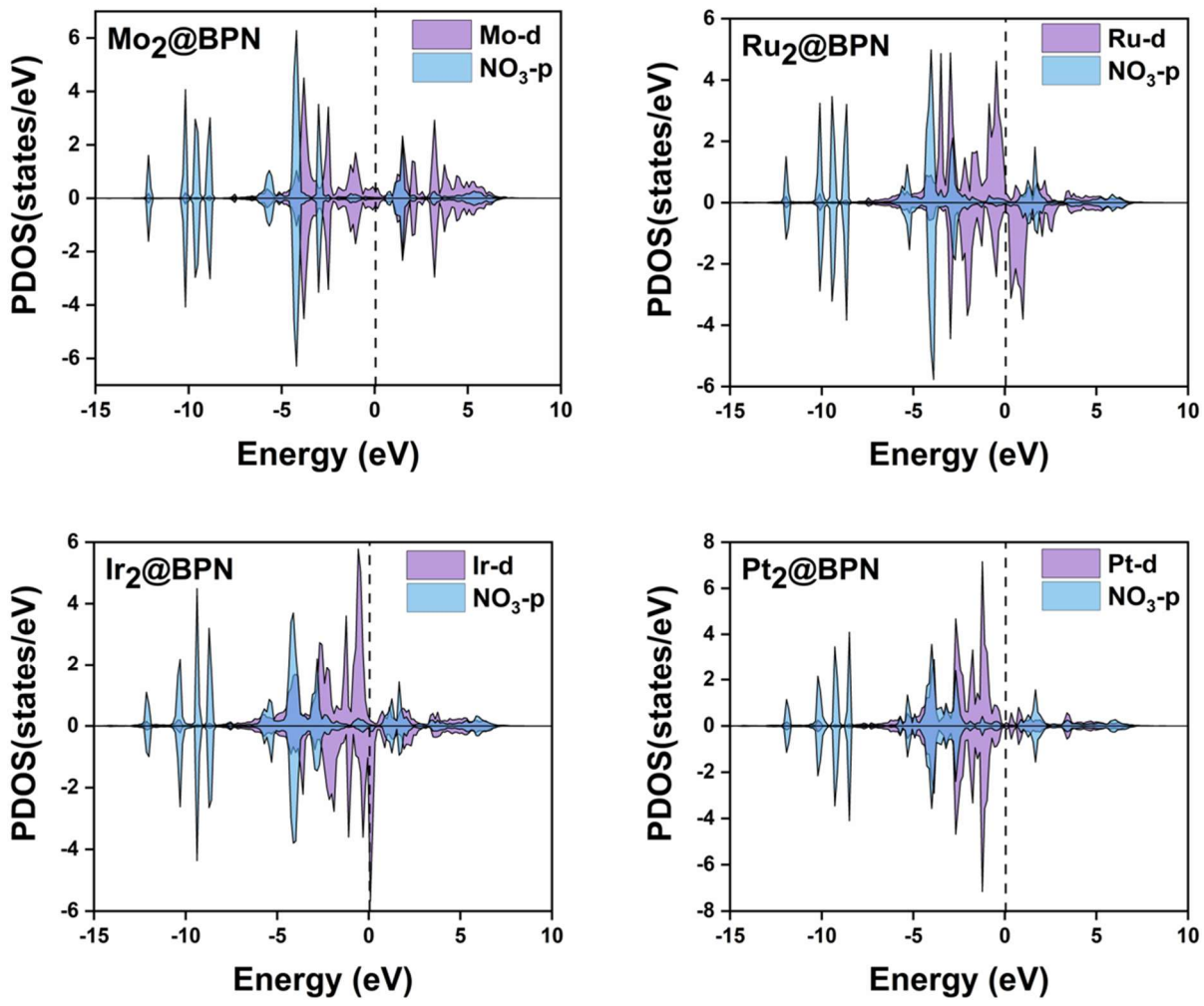

Figure S17. Partial density of states (PDOS) on the molecular orbital of NO_3 and the d orbital of metal atoms on Mo_2@BPN, Ru_2@BPN, Ir_2@BPN and Pt_2@BPN catalysts after NO_3 adsorption.

(a)

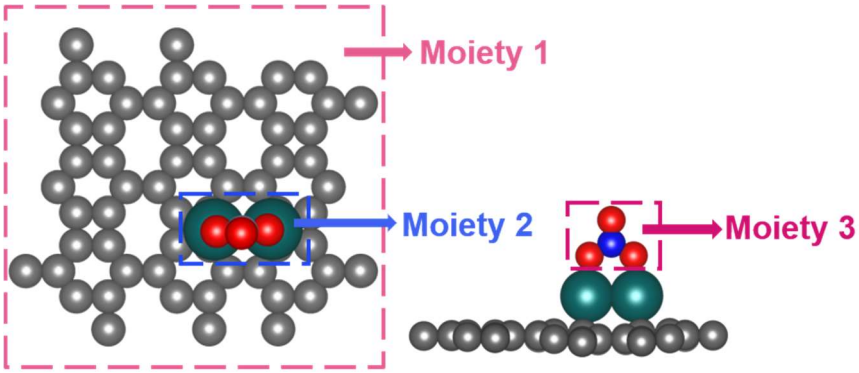

(b)

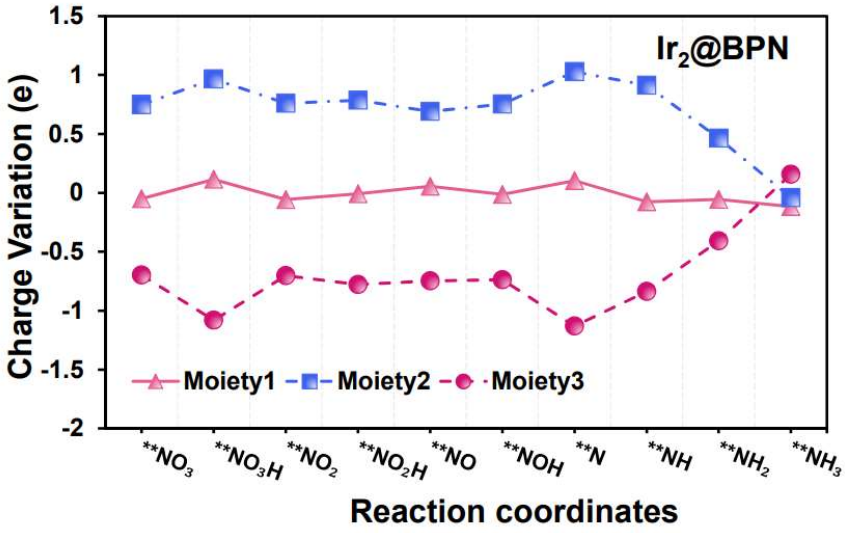

Figure S18. **(a)** Three moieties of TM_2@BPN. **(b)** Charge variation during the process of NO_3RR on Ir_2@BPN.

(a)

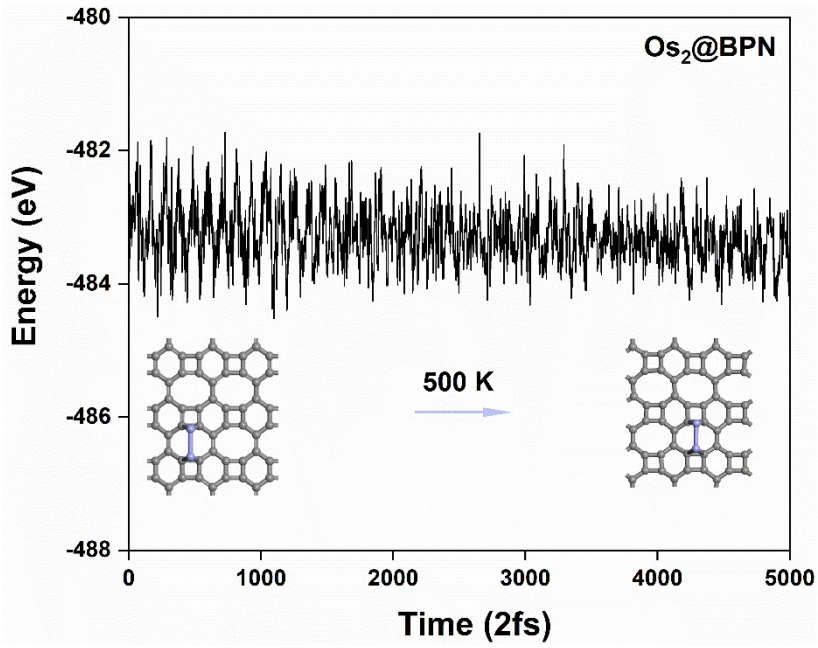

(b)

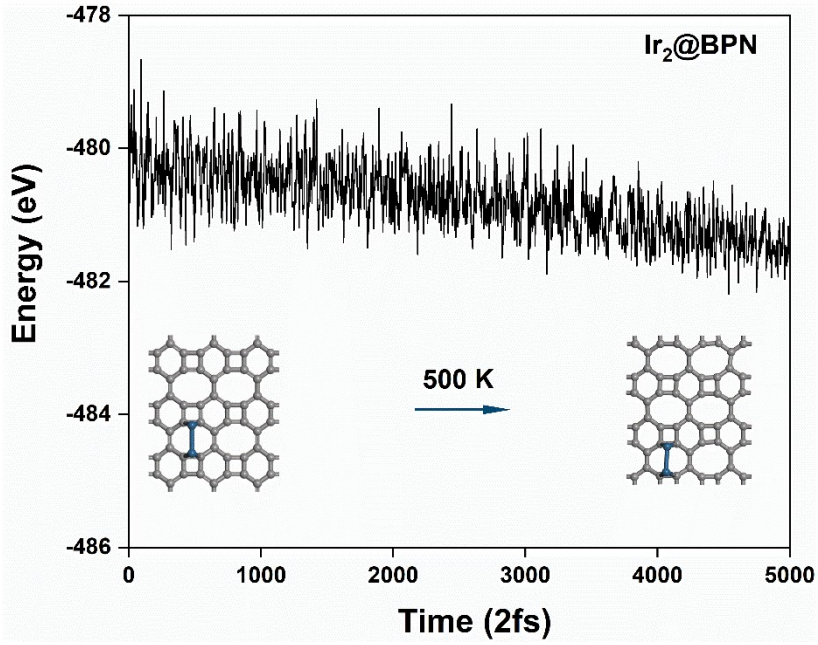

Figure S19. Ab initio molecular dynamics simulation of **(a)** Os_2@BPN, and **(b)** Ir_2@BPN was carried out at 500 K for a total duration of 10 ps with a time step of 2 fs.

Table S1. Zero-point energy (ΔE_{ZPE}) and entropy ($T\Delta S$) at room temperature of gaseous molecules from the NIST database.

Species	E_{ZPE}	$T\Delta S$
HNO_3	0.69	0.83
H_2	0.27	0.41
NH_3	0.91	0.59
H_2O	0.58	0.67
NO_2	0.23	0.74
NO	0.12	0.64

Table S2. The computed binding energy **(E_b)**, cohesive energy **(E_{coh})** and the difference between binding and cohesive **(E_b-E_{coh})** of TM dimers in TM_2@BPN.

Metal	E_b (eV)	E_{coh} (eV)	E_b-E_{coh} (eV)
Sc_2	-7.85	-5.27	-2.58
Ti_2	-7.22	-6.21	-1.01
V_2	-5.33	-5.60	0.02
Cr_2	-2.90	-4.19	1.03
Mn_2	-4.48	-4.62	0.14
Fe_2	-8.56	-7.43	-1.13
Co_2	-4.88	-5.14	0.12
Ni_2	-5.89	-4.96	-0.93
Cu_2	-2.91	-3.73	0.53
Zn_2	-0.07	-1.00	0.93
Y_2	-7.81	-4.75	-3.05
Zr_2	-9.28	-7.03	-2.25
Nb_2	-8.10	-6.94	-1.15
Mo_2	-7.28	-6.42	-0.86
Ru_2	-8.85	-8.16	-0.69
Rh_2	-6.85	-5.80	-1.05
Pd_2	-4.46	-3.74	-0.72
Ag_2	-1.77	-2.82	0.72
Cd_2	-0.08	-0.62	0.54
Hf_2	-9.31	-7.31	-1.99
Ta_2	-9.87	-8.56	-1.31
W_2	-9.62	-8.88	-0.74
Re_2	-7.60	-7.85	0.25
Os_2	-8.74	-8.71	-0.03
Ir_2	-8.07	-7.18	-0.88
Pt_2	-7.02	-5.43	-1.58
Au_2	-2.58	-3.09	0.51
Hg_2	-0.06	-0.20	0.14

Table S3. Electronic and structural properties of TM_2@BPN, including TM dimer bond length **(d_{M-M})**, charge transfer **(CT)** from TM dimer to substrate, and d band center **(ε_d)**.

Metal	d_{M-M} (Å)	CT (e)	ε_d (eV)
Sc_2	4.07	3.27	2.24
Ti_2	3.77	2.95	0.57
V_2	2.43	1.98	0.51
Mn_2	2.56	1.28	-0.96
Fe_2	2.18	0.94	-1.89
Co_2	2.17	0.69	-2.32
Ni_2	2.35	0.61	-2.29
Y_2	4.09	2.57	3.42
Zr_2	3.55	2.34	2.02
Nb_2	2.60	1.72	0.76
Mo_2	1.72	0.95	-1.73
Ru_2	2.25	0.65	-2.61
Rh_2	2.62	0.52	-2.37
Pd_2	2.65	0.29	-3.95
Hf_2	3.28	4.41	1.90
Ta_2	2.48	2.89	0.69
W_2	2.10	1.39	-0.03
Re_2	2.13	0.99	-1.77
Os_2	2.27	0.69	-2.64
Ir_2	2.40	0.35	-3.39
Pt_2	2.55	0.16	-4.58

Table S4. Calculated adsorption free energy ΔG_{*NO3} (eV) on TM_2@BPN, via (η^1-O-1), (η^2-O-1) and (η^2-O-2) configuration.

Metal	(η^1-O-1)	(η^2-O-1)	(η^2-O-2)
Sc_2	-1.43	-2.39	-2.96
Ti_2	-1.67	---	-3.20
V_2	-1.62	Relax to η^2-O-2	-2.80
Mn_2	-0.57	Relax to η^2-O-2	-2.12
Fe_2	Relax to η^2-O-2	Relax to η^2-O-2	-1.83
Co_2	Relax to η^2-O-2	Relax to η^2-O-2	-1.88
Ni_2	Relax to η^2-O-2	Relax to η^2-O-2	-1.68
Y_2	-1.45	-2.15	-2.87
Zr_2	-1.52	-2.20	-2.81
Nb_2	-1.14	Relax to η^2-O-2	-2.51
Mo_2	-0.87	Relax to η^2-O-2	-2.11
Ru_2	Relax to η^2-O-1	-0.89	-1.39
Rh_2	Relax to η^2-O-2	Relax to η^2-O-2	-1.52
Pd_2	-0.38	-0.69	-0.77
Hf_2	-1.64	---	-3.08
Ta_2	-1.53	---	-2.88
W_2	Relax to η^1-O-2	---	-2.60
Re_2	-1.22	Relax to η^2-O-2	-2.13
Os_2	-6.78	-0.82	-1.21
Ir_2	-0.10	-0.37	-1.04
Pt_2	Relax to η^2-O-2	Relax to η^2-O-2	-0.91

Table S5. Transition Metal to Oxygen bond distance for the stable NO_3^- adsorbed configuration (η^2-O-2) on TM_2@BPN.

Metal	dM_1-O_1 (Å)	dM_2-O_2 (Å)
Sc_2	2.10	2.08
Ti_2	1.97	1.97
V_2	1.96	1.96
Mn_2	1.95	1.94
Fe_2	1.92	1.92
Co_2	1.89	1.89
Ni_2	1.88	1.89
Y_2	2.25	2.22
Zr_2	2.14	2.15
Nb_2	2.13	2.11
Mo_2	2.12	2.13
Ru_2	2.07	2.07
Rh_2	2.06	2.03
Pd_2	2.12	2.11
Hf_2	2.08	2.07
Ta_2	2.04	2.05
W_2	2.03	2.03
Re_2	2.04	2.04
Os_2	2.07	2.06
Ir_2	2.05	2.09
Pt_2	2.09	2.09

Table S6. Calculated Gibbs free energy of *H (ΔG_{*H}) adsorption on TM_2@BPN.

Metal	ΔG_{*H} (eV)
Sc_2	0.43
Ti_2	-1.06
V_2	-1.52
Mn_2	-1.002
Fe_2	-0.69
Co_2	-0.89
Ni_2	-0.85
Y_2	-0.88
Zr_2	-0.53
Nb_2	-1.17
Mo_2	-0.50
Ru_2	-0.39
Rh_2	-1.02
Pd_2	-0.44
Hf_2	-0.86
Ta_2	-1.17
W_2	-0.39
Re_2	-0.75
Os_2	-0.66
Ir_2	-0.58
Pt_2	-0.27

Table S7. Calculated charge transfer (CT) from TM dimer to NO_3, on TM_2@BPN.

Metal	CT (e)
Sc_2	-1.03
Ti_2	-1.13
V_2	-0.97
Mn_2	-0.87
Fe_2	-0.88
Co_2	-0.73
Y_2	-0.97
Zr_2	-0.99
Nb_2	-0.89
Mo_2	-0.90
Ru_2	-0.76
Rh_2	-0.74
Pd_2	-0.73
Hf_2	-1.09
W_2	-1.09
Re_2	-0.93
Os_2	-0.80
Ir_2	-0.69
Pt_2	-0.68

Table S8. The Computed limiting potential (U_L) and potential determining step (PDS) of TM_2@BPN for NO_3RR.

Metal	U_L (V)	PDS
Sc_2	-2.19	*OH → *OH_2
Ti_2	-1.92	*OH → *OH_2
V_2	-1.57	*OH → *OH_2
Mn_2	-0.86	*NH_2 → *NH_3
Fe_2	-0.75	*NH_2 → *NH_3
Co_2	-1.69	*OH → *OH_2
Ni_2	-0.59	*NH_2 → *NH_3
Y_2	-2.3	*OH → *OH_2
Zr_2	-2.06	*OH → *OH_2
Nb_2	-1.87	*OH → *OH_2
Mo_2	-0.40	*NO_2→ *OH-*NO
Ru_2	-0.36	*NH_2 → *NH_3
Rh_2	-0.16	**NO→**NOH
Pd_2	-0.56	*NO_2→ *OH-*NO
Hf_2	-1.75	*OH → *OH_2
Ta_2	-1.79	*NH_2OH → *OH
W_2	-1.29	*NH_2OH → *OH
Re_2	-1.10	*OH → *OH_2
Os_2	-0.32	*NO→*NOH
Ir_2	-0.35	*NH_2 → *NH_3
Pt_2	-0.45	*NO_2→ *OH-*NO

Table S9. The calculated Zero-point energy (ΔE_{ZPE}) and entropic contributions ($T\Delta S$) at room temperature (298.15 K) to the Gibbs free energies of each elementary step for Rh_2@BPN. The unit is eV.

Reaction Intermediate	ZPE	$T\Delta S$
***NO_3**	0.411886356	0.237674
***NO_3H**	0.594182189	0.36836
***NO_2**	0.246676255	0.192045
***NO_2H**	0.528059538	0.285605
***NO**	0.174623183	0.180012
***NOH**	0.478887257	0.120561
***NHOH**	0.687736906	0.194516
***NH_2OH**	0.989150923	0.279013
***NH_2**	0.688463775	0.120496
***NH_3**	0.972807823	0.201186

Table S10. The calculated Zero-point energy (ΔE_{ZPE}) and entropic contributions ($T\Delta S$) at room temperature (298.15 K) to the Gibbs free energies of each elementary step for Os_2@BPN. The unit is eV.

Reaction Intermediate	ZPE	$T\Delta S$
***NO_3**	0.407854772	0.23698396
***NO_3H**	0.598977333	0.33509831
***NO_2**	0.269120928	0.17842331
***NO_2H**	0.47364532	0.32699135
***NO**	0.183149329	0.15536326
***NOH**	0.47166756	0.15971709

***N**	0.092907907	0.04237797
***NH**	0.360087728	0.07510918
***NH_2**	0.710595576	0.08048906
***NH_3**	1.029020916	0.17182477

Table S11. The calculated Zero-point energy (ΔE_{ZPE}) and entropic contributions ($T\Delta S$) at room temperature (298.15 K) to the Gibbs free energies of each elementary step for Ir_2@BPN. The unit is eV.

Reaction Intermediate	ZPE	$T\Delta S$
***NO_3**	0.4105032	0.2444296
***NO_3H**	0.57244292	0.4347727
***NO_2**	0.27766138	0.1789226
***NO_2H**	0.5118728	0.2985911
***NO**	0.16876833	0.1847541
***NOH**	0.46187944	0.1865558
***N**	0.08414371	0.0785057
***NH**	0.34859161	0.1056357
***NH_2**	0.70977985	0.0869787
***NH_3**	1.02871144	0.1976006

Table S12. Calculated adsorption free energy ΔG_{*NO} (eV) on TM_2@BPN, via *NO end, *ON end, and **NO side configurations.

Metal	*NO-end	*ON-end	**NO-side
Sc_2	Relax to NO-side	Relax to NO-side	-5.82
Ti_2	Relax to NO-side	Relax to NO-side	-6.90
V_2	Relax to NO-side	-4.41	-7.24
Mn_2	-5.27	-3.69	-5.71
Fe_2	Relax to NO-side	-3.74	-5.69
Co_2	Relax to NO-side	-3.62	-6.23
Ni_2	-4.51	Relax to NO-side	-5.32
Y_2	-5.77	Relax to NO-side	-6.51
Zr_2	-5.23	Relax to NO-side	-7.46
Nb_2	Relax to NO-side	-4.13	-7.25
Mo_2	-4.83	-3.29	-4.33
Ru_2	Relax to NO-side	-3.07	-5.03
Rh_2	Relax to NO-side	-3.41	-5.35
Pd_2	-3.94	Relax to NO-end	-4.10
Hf_2	Relax to NO-side	Relax to NO-side	-7.56
Ta_2	Relax to NO-side	Relax to NO-side	-7.72
W_2	-5.38	-3.56	-6.05
Re_2	-4.73	-2.91	-4.90
Os_2	-4.85	-2.34	-4.54
Ir_2	-4.96	-2.61	-4.83
Pt_2	-3.86	-2.88	-4.04

Table S13. Calculated adsorption free energy ΔG_{*NO3} (eV) on TM@BPN, via 1-O, and 2-O configuration.

Metal (SACs)	1-O	2-O
Rh	-0.17	-0.96
Os	-1.12	-1.81
Ir	-0.89	-1.63

Table S14. The comparison of catalytic performance (reflected by limiting potential, U_L) for Nitrate reduction reaction on various electrocatalysts.

Electrocatalysts	U_L (V)	References
Fe-V_2O_5	-0.37	1
BiPd	-0.40	2
FeB_2	-0.31	3
RuOx	-0.33	4
Ni-Cu-SSA	-0.33	5
10Cu/TiO_{2-x}	-1.18	6
Cu-*cis*-N_2O_2	-0.39	7
WSe_{2-x}	-0.86	8
Fe-SnS_2-Vs	-3.04	9
FeS_2	-0.71	10
Rh_2@BPN	-0.16	This work
Os_2@BPN	-0.32	This work
Ir_2@BPN	-0.35	This work

Table S15. Calculated d-band center **(ε_d)** of TM@BPN.

Metal (SACs)	ε_d (eV)
Rh	-3.26
Os	-2.50
Ir	-3.05

Table S16. Calculated limiting potential of HER and NO_3RR and faradic efficiency (FE) values for TM_2@BPN.

Metals	$U_L(NO_3RR)$	$U_L(HER)$	FE%
Mo_2	-0.40	-0.50	98.0
Ru_2	-0.36	-0.39	78.8
Rh_2	-0.16	-0.69	100.0
Os_2	-0.32	-0.41	99.9
Ir_2	-0.35	-0.39	99.9
Pt_2	-0.45	-0.27	0.09

Table S17. Comparison of nitrate reduction reaction pathways on the Rh_2@BPN by using DFT-D3 and DFT-Sol method.

Rh	NO_3	1	2	3	4	5	6	7	8	9	U_L
DFT-D3	-1.525	-2.877	-4.069	-5.479	-5.353	-5.188	-5.535	-6.598	-7.234	-7.188	0.16
DFT-D3-Sol	-1.371	-2.861	-3.916	-5.329	-5.088	-5.011	-5.383	-6.450	-7.103	-7.410	0.24

Table S18. Comparison of nitrate reduction reaction pathways on the Os_2@BPN by using DFT-D3 and DFT-Sol method.

Os	NO_3	1	2	3	4	5	6	7	8	9	U_L
DFT-D3	-1.208	-4.093	-3.827	-4.318	-4.852	-4.527	-6.398	-6.840	-6.991	-7.079	0.32
DFT-D3-Sol	-1.209	-4.184	-3.851	-4.402	-4.915	-4.629	-6.434	-6.834	-7.133	-7.487	0.29

Reference

1. N. Zhang, G. Zhang, P. Shen, H. Zhang, D. Ma and K. Chu, Adv. Funct. Mater., 2023, 33, 2211537.

2. K. Chen, Z. Ma, X. Li, J. Kang, D. Ma and K. Chu, Adv. Funct. Mater., 2023, 33, 2209890.

3. G. Zhang, X. Li, K. Chen, Y. Guo, D. Ma and K. Chu, Angew. Chem. Int. Ed., 2023, 62, e202300054.

4. X. Li, P. Shen, X. Li, D. Ma and K. Chu, ACS Nano, 2023, 17, 1081-1090.

5. J. Cai, Y. Wei, A. Cao, J. Huang, Z. Jiang, S. Lu and S.-Q. Zang, Appl. Catal. B: Environ., 2022, 316, 121683.

6. X. Zhang, C. Wang, Y. Guo, B. Zhang, Y. Wang and Y. Yu, J. Mater. Chem. A., 2022, 10, 6448-6453.

7. X.-F. Cheng, J.-H. He, H.-Q. Ji, H.-Y. Zhang, Q. Cao, W.-J. Sun, C.-L. Yan and J.-M. Lu, Advanced Materials, 2022, 34, 2205767.

8. P. Shen, G. Wang, K. Chen, J. Kang, D. Ma and K. Chu, J. Colloid Interface Sci., 2023, 629, 563-570.

9. K. Chen, Y. Luo, P. Shen, X. Liu, X. Li, X. Li and K. Chu, Dalton Transactions, 2022, 51, 10343-10350.

10. N. Zhang, G. Zhang, Y. Tian, Y. Tang and K. Chu, Dalton Transactions, 2022, 51, 16805-16810.